

Article

# Adjusting Electric Field Intensity Using Hybridized Dielectric Metamolecule

Haohua Li , Xiaobo Wang  and Ji Zhou \*

State Key Laboratory of New Ceramics and Fine Processing, School of Materials Science and Engineering, Tsinghua University, Beijing 100084, China; lhh14@mails.tsinghua.edu.cn (H.L.); wangxb14@mails.tsinghua.edu.cn (X.W.)

\* Correspondence: zhouji@mail.tsinghua.edu.cn

Received: 15 August 2019; Accepted: 8 October 2019; Published: 14 October 2019



**Abstract:** In this paper, we report on achieving the hybridization effect in a Mie-based dielectric metamolecule and provide its physically intuitive picture. Hybridization results in the splitting of the initial overlapping resonance dips, thus leading to two new collective resonance modes. It was observed via the simulated displacement field distribution that the two modes behave as the in-phase and out-of-phase oscillation of two meta-atoms, thus enhancing and suppressing the intensity of the electric field at the gap between two meta-atoms. Moreover, since the two hybridized modes are caused by the interaction effect, the intensities of the electric field can be adjusted by several external factors, like applied forces and temperature. Taking advantage of this easy-equipped dielectric meta-device, certain zones in it can be applied to receive amplified signals and shielded noises of different frequencies in microwave communication fields. Moreover, due to the function of enhancing electric field intensities, it is also promising in wireless charging technology.

**Keywords:** metamolecule; hybridization effect; enhanced and suppressed fields; tailorable

## 1. Introduction

Veselago put forward the concept of double-negative material from the Maxwell equation in 1967 [1], and theoretically predicted a series of novel electromagnetic behaviors [2–5]. Since the size of the single unit and separation between unit cells within a metamaterial are smaller than the working wavelength, the interaction between meta-atoms initiates the near-field hybridization phenomenon and corresponding applications [6–10]. Inspired by the molecular orbital diagram and energy level theory, scientists have developed various hybridization models to explain the energy level splitting of a coupled system [11–14]. Halas and Nordlander first introduced the hybridization model to the nanoshell structure [7], whose resonance frequency can be attributed to the interaction of a nanosphere and a nanocavity. Verellen proposed an assembled gold nanocross cavity structure using a nanocross and a nanorod. Owing to the interference of the two elements, the resonance of the assembled structure hybridizes into a bonding quadrupolar mode and a subradiant bonding dipolar mode [15]. Hybridized modes in metamolecules usually lead to enhanced electric fields, thus bringing out various applications, such as improved fluorescence emission [16], and surface-enhanced Raman scattering [17,18]. Pablo Alonso-González demonstrated an infrared dimer nanoantenna producing enhanced and suppressed electric fields in hybridized modes [19]. Rostam Moradian proposed a bimetallic core-shell structure to realize surface enhanced Raman scattering by means of hybridized resonance modes [20].

However, most coupling hybridization models focus on optical and terahertz wavelengths [9,10,12,21–25]. In comparison, hybridization in microwaves have special applications in communication fields, such as receiving signals, and collecting electric energy. Moreover, compared to

metallic structures, dielectric metamaterials have the advantages of low losses, simple structures and active regulation [26–30].

Here, we discuss a hybridization model in a microwave band composed of dielectric meta-atoms. Hybridization between two dielectric meta-atoms with the same Mie resonance frequencies results in an interaction, which leads to a transparent window together with two new collective resonance modes. Dielectric materials produce the first-order Mie resonance by excitation of a microwave, behaving as a magnetic dipole formed by displacement current loops. In the two collective modes, the displacement current oscillated as the in-phase mode and out-of-phase mode in two meta-atoms, respectively, strengthened and weakened the electric fields between them. Utilizing constructive or destructive interaction, the simulated electric field intensities were enhanced or suppressed compared with the incident fields. Moreover, the intensities of electric fields can be tuned by adjusting several factors that affect the coupling effect, like the gap distances and permittivities of meta-atoms. The metamolecule with enhancing or weakening electric fields can be served to receive amplified or shielded signals at certain bands, which is promising in microwave communication fields. This meta-device can also be applied as a harvester to collect electric energy from propagating electromagnetic waves at a specific frequency, which is promising in wireless charging technology.

## 2. Design and Performance

As Figure 1 shows, the dielectric metamolecule is composed of  $\text{CaTiO}_3$  (CTO) and  $\text{SrTiO}_3$  (STO) meta-atoms, shaped into cuboids. The complex permittivities of  $\text{CaTiO}_3$  and  $\text{SrTiO}_3$  are  $\epsilon_r = 160$ ,  $\tan\delta = 0.001$  and  $\epsilon_r = 317$ ,  $\tan\delta = 0.003$ , respectively. The dimensions of the CTO and STO meta-atoms were carefully designed to be  $2 \times 1.8 \times 2 \text{ mm}^3$  and  $1 \times 2 \times 2 \text{ mm}^3$ , respectively, which matches with their permittivity so that the frequencies of their first-order Mie resonance are nearly the same. Together, permittivity and dimension determine the frequency of the first-order Mie resonance according to Equation (1):

$$f = \frac{\theta c}{2\pi r \sqrt{\epsilon \mu'}} \quad (1)$$

where  $\theta$  is a coefficient that approximates to  $\pi$ ,  $c$  is light velocity in a vacuum,  $\mu$  equals to 1 for non-magnetic materials, and  $r$  and  $\epsilon$  represent the radius and permittivity of the dielectric sphere.

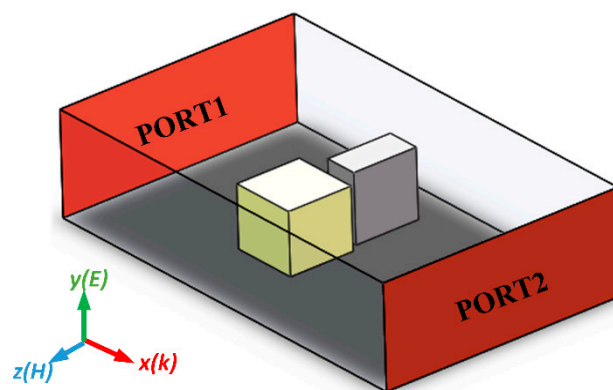


**Figure 1.** Schematic diagram of the metamolecule in a waveguide. The two meta-atoms are arranged side-by-side along the  $z$ -axis, being symmetric to  $y$ - $z$  plane and  $x$ - $z$  plane. The incident wave propagates along the  $x$ -axis, the magnetic field and the electric field are along the  $z$ -axis and  $y$ -axis, respectively.

Simulations are performed using the commercial software package CST (Computer Simulation Technology) to calculate the transmission spectra of both the single meta-atoms and the assembled metamolecule. As the dashed curves in Figure 2a show, the two meta-atoms produce dramatic transmission dips at similar frequencies around 10.48 GHz for an incident electromagnetic wave. As such, the two dips nearly overlap. This means that the meta-atoms with their specifically designed

dimensions and permittivities are opaque to the incident electromagnetic wave at a coincidental frequency. The displacement electric currents at the resonance frequency oscillate inside dielectric cuboids, forming a magnetic dipole, which indicates that the first-order Mie resonances occurs at a nearly overlapping frequency. The metamolecule described in Figure 1 shows two meta-atoms arranged side-by-side along the  $z$ -axis, parallel to the magnetic field of the incident wave. The distance between the two meta-atoms is 0.60 mm, which is much smaller than the working wavelength. Thus, the coupling between the two meta-atoms is strong enough to induce the redistribution of displacement electric fields in the metamolecule. The solid curves in Figure 2a show the transmission response ( $S_{21}$ ) of the metamolecule at 9.50–11.00 GHz. It can be seen that a typical hybridization induced transparency (HIT) phenomenon appears. An electromagnetic transparent window replaces the original intrinsic resonance dips of the meta-atoms. In addition, two new transmission dips of the metamolecule emerge at 10.16 GHz and 10.73 GHz. It is worth mentioning that the amplitudes of the two dips are  $-15.02$  dB and  $-1.16$  dB, while the metamolecule becomes transparent with an amplitude of  $-0.24$  dB at 10.48 GHz.

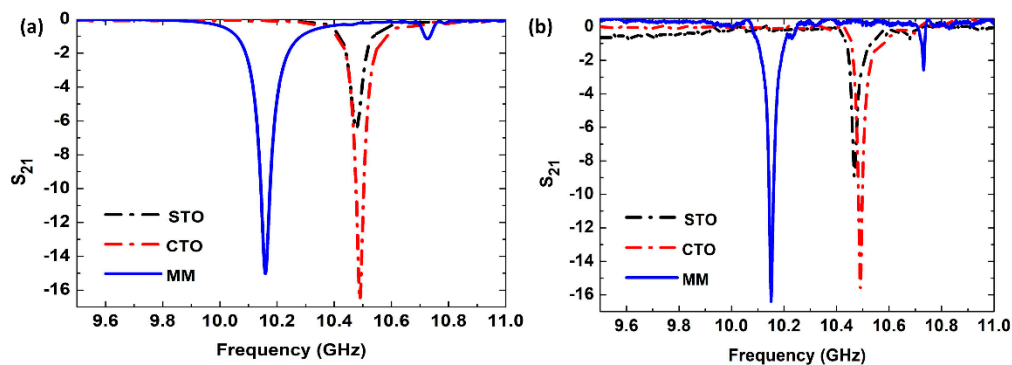


**Figure 2.** Simulated (a) and measured (b)  $S_{21}$  curves of CTO and STO meta-atoms (dashed lines) and the metamolecule (solid lines). MM is the abbreviation of metamolecule.

The  $S_{21}$  curves are measured by a microwave system. Samples of ceramic  $\text{CaTiO}_3$  (CTO) and  $\text{SrTiO}_3$  (STO) are cut into cuboids with a size of  $2 \times 1.8 \times 2 \text{ mm}^3$  and  $1 \times 2 \times 2 \text{ mm}^3$ . They are placed at the center of the XB-SW90 rectangular waveguide carefully, with gap of 0.60 mm to form the metamolecule. The waveguides are connected to the Agilent N5230C vector network analyzer by coaxial lines. The electromagnetic wave at 9.5–11.0 GHz propagates from port 1 to port 2 through the waveguide and thus the transmission spectra are obtained. At the center of the waveguide, where the metamolecule is placed, the electromagnetic environment is as the simulated one, which means that the direction of propagations, electric fields and magnetic field of EM-waves are perpendicular to each other. The dashed curves in Figure 2b show the transmission spectra of the meta-atoms. The transmission dips of the CTO and STO cuboids appear at 10.49 GHz and 10.47 GHz, respectively, and agree well with the results of the simulation. The solid curves in Figure 2b depict the transmission spectra of the metamolecule. Two dips can be seen at 10.15 GHz and 10.73 GHz. These findings agree well with the results obtained from the simulation.

### 3. Discussion

Since the metamolecule is composed of dielectric meta-atoms, their first-order Mie resonance is caused by displacement electric current loops. To fully explore the mechanism behind the phenomenon of hybridization induced transparency (HIT), the distribution of the displacement electric field of the metamolecule is calculated at the frequencies of both the collective resonance dips and the transparent window. Figure 3 shows the displacement electric fields of the cross sections of both meta-atoms on the  $x$ - $y$  plane. As Figure 3a shows, at the red-shifted collective resonance dip of 10.16 GHz in the simulation, two magnetic dipoles appear in both meta-atoms. These dipoles oscillate in a parallel

direction and are found to be in an in-phase mode. Another collective mode of the metamolecule is blue-shifted to 10.73 GHz and is visible as a slight dip. As Figure 3b shows, the displacement fields in the two meta-atoms oscillate in anti-parallel directions and are therefore considered as an out-of-phase mode. Because it is weakened by the counteracting effect of the anti-parallel oscillation, the amplitude of the resonance at 10.73 GHz is much weaker than the former one. As for the initial resonance frequency of the meta-atoms at ca. 10.48 GHz, it can be seen from Figure 3c that the electric fields are mostly not localized in dielectrics and spread in space. As a result, electromagnetic transparency is induced.

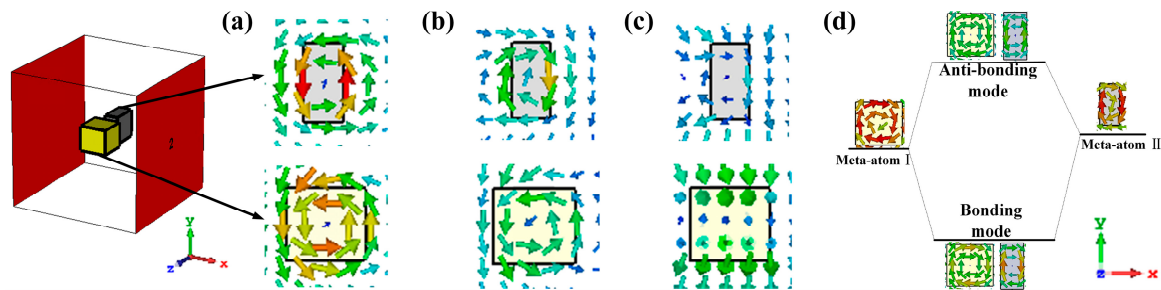


**Figure 3.** Electric field distribution in the metamolecule at (a) 10.16 GHz, (b) 10.73 GHz and (c) 10.48 GHz. The illustrations show the electric field of each meta-atom on the central cross section of  $z = 1.3$  mm and  $z = -1.3$  mm, respectively, which are perpendicular to  $z$ -axis. The first line represents the central cross section of the STO meta-atom, and the second line represents the CTO meta-atom. (d) Resonance hybridization picture of the metamolecule with an electric field distribution at each resonance frequency.

Like “heteronuclear diatomic molecules” and their constituents, the proposed mechanism can be viewed as a hybridization model for the dielectric metamolecule, as described in Figure 3d. Meta-atoms initially share the same Mie resonance frequency due to their intrinsic properties. Owing to the strong coupling effect, interaction occurs at their overlapping orbits. The metamolecule generates new collective orbits, which displays as two new resonance dips. Coupled meta-atoms are combined as modified “dielectric diatomic molecules”. The red-shifted and blue-shifted collective modes can be regarded as a low-energy “bonding” mode and a high-energy “anti-bonding” mode.

From the hybridization model of a dielectric metamolecule, it can be seen that both meta-atoms produce strong Mie resonance in collective modes. However, due to the strengthening and weakening effect of the in-phase and out-of-phase oscillation, it can be inferred that the intensities of electric fields are enhanced and suppressed between two meta-atoms accordingly, especially in their gap region. The simulated intensities of the electric field in plane  $y = 0$  at two collective resonance frequencies are shown in Figure 4a,b. Both the meta-atoms have strong localized electric fields inside. However, due to the different interactions of the two modes, their radiated fields are superimposed and counteracted, respectively. We have calculated the intensity of the electric fields on the central axis between two meta-atoms, as shown in Figure 4c,d. For the first red-shifted collective mode, the intensity of the electric field has been enhanced generally by four to five times in most regions on the central axis compared to the incident electric field. Whereas for the second blue-shifted collective mode, the intensity of the electric field on the central axis has been diminished to zero to 0.7 times compared to the incident one. This corroborates with our hybridization model of the dielectric metamolecule. Since most electric fields are localized inside two meta-atoms and the out-of-phase oscillation of the displacement current impels the counteracting of the radiated fields at the gap between two meta-atoms, the electric fields are weakened compared to the incident fields. Certain zones between meta-atoms in two collective modes can be regarded as an “enlarged zone” and a “diminished zone” at a corresponding frequency, which induces enhanced or diminished electric fields.

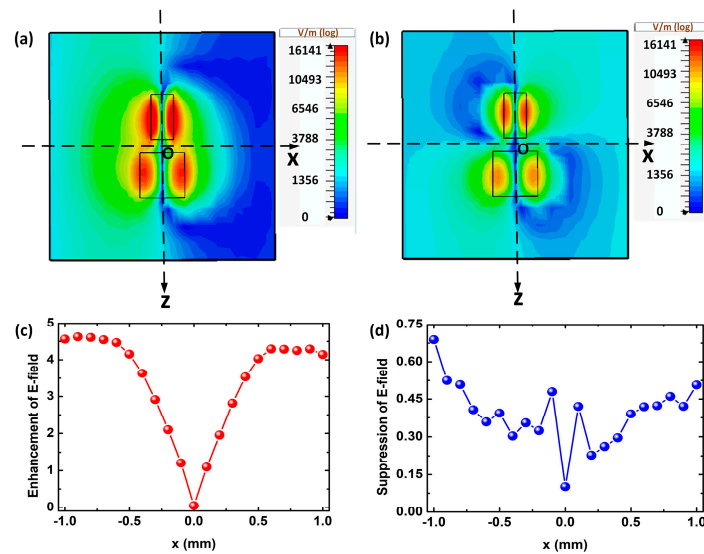


**Figure 4.** The simulated electric field intensity of the metamolecule at (a) 10.16 GHz and (b) 10.73 GHz. (c) Electric field enhancement  $|E|/|E_0|$  at 10.16 GHz and (d) electric field reduction  $|E|/|E_0|$  at 10.73 GHz on the central axis ( $y = z = 0$ ) with  $x$  changes from  $-1$  to  $1$  mm, where  $|E_0|$  represents for the incident electric intensity.

By utilizing the collective mode of the metamolecule, we can obtain enhanced or diminished electric fields at certain spatial zones. Since the collective mode results from the coupling hybridization effect, factors that affect coupling strength can be used to adjust the response of the metamolecule, thus tailoring the enhancement and suppression amplitudes of the electric fields.

Distances between two meta-atoms strongly affect the coupling strength of the metamolecule. In order to adjust the distance between two meta-atoms, a flexible substrate is used to bond the two meta-atoms together. Thus, external forces can be applied to change gap distances between two meta-atoms from  $0.9$  mm to  $0.1$  mm. The simulated and measured  $S_{21}$  curves of the metamolecule with different gap distances are shown in Figure 5a,b. The simulated intensity of the  $E$ -field at a fixed point  $(-0.8, 0, 0)$  of these gap distances are shown in Figure 5c. The intensity is increasingly enhanced as the gap between two meta-atoms decreases. When the gap is  $0.1$  mm, the first collective mode resonates at  $9.79$  GHz, where the enhancement amplitude of electric field intensity reaches up to  $7.4$  times compared with the incident electric field. It can be seen that the coupling becomes stronger with decreasing gap distance, inducing greater electric intensity at  $(-0.8, 0, 0)$ , which is one point in the spatial gap region. As for the second collective mode, the suppression degree is at its greatest at  $0.54$  when the gap distance is  $0.1$  mm. It is worth mentioning that the two discontinued points in Figure 5c are caused by the adaptive mesh division in the simulation.

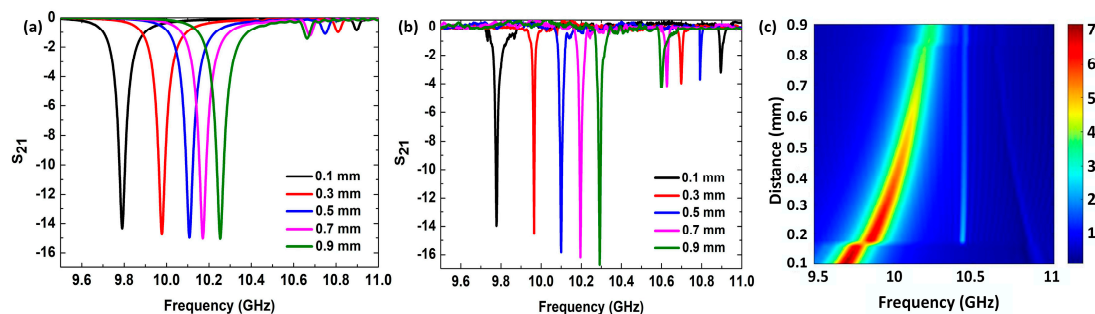


**Figure 5.** (a) Simulated and (b) measured  $S_{21}$  curves of the metamolecule with different gap distances. (c) Simulated electric field enhancement  $|E|/|E_0|$  at point  $(-0.8, 0, 0)$  with gap distances decreasing from  $0.9$  mm to  $0.1$  mm at  $9.50$ – $11.00$  GHz.

Temperature also has a great influence on the enhancement degree in certain zones at the first collective mode. As Figure 6a shows, the  $S_{21}$  curves of the metamolecule are simulated under increasing temperatures from 298 K to 418 K with a step of 40 K. To verify our simulation results, heating belts and temperature controllers were used to adjust the temperature of the sample from 298 K to 418 K, as shown in Figure 6b. Transmission curves are more asymmetrical as temperature increases. This results from the different temperature coefficients of dielectric constant of the two meta-atoms. The thermo-effect leads to greater differences in permittivity of the two meta-atoms, thus inducing the separation of the resonance dips of the two meta-atoms. The separation of the resonance dips of the two meta-atoms results in greater asymmetry of the metamolecule. The simulated enhancement amplitudes in the first collective mode of the metamolecule at different temperatures are shown in Figure 6c. It can be seen that the enhancement becomes weaker as the asymmetric degree increases. Therefore, it can be concluded that the enhancement reaches its peak when the metamolecule is most symmetric.

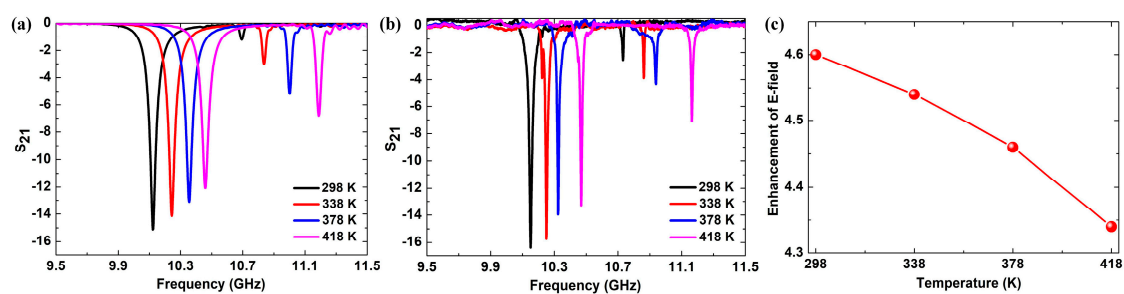


**Figure 6.** (a) Simulated and (b) measured  $S_{21}$  curves of the metamolecule at different temperatures. (c) Simulated electric field enhancement  $|E|/|E_0|$  at point  $(-0.8, 0, 0)$  when temperature rises from 298 K to 418 K with a step of 40 K, where  $|E_0|$  represents the incident electric intensity,  $|E|$  represents the electric intensity at the first collective resonance frequency of the metamolecule.

#### 4. Conclusions

In this study, hybridization of the dielectric metamolecule induces a transparent window while two new collective modes appear. At the frequencies of the two collective modes, displacement currents are distributed as loops with in-phase and out-of-phase oscillation in two meta-atoms. The superimposition and counteracting interactions result in the strengthening and weakening effects of electric fields. Moreover, the enhancement amplitudes can be adjusted via coupling factors, behaving as a steerable meta-device. Due to the enhancement effect and diminishment effect in corresponding collective modes, the metamolecule can be used to amplify signals or shield noises in microwave communication and because of the enhancement of electric field intensities, it is also promising to harvest electric energy from propagating electromagnetic waves in specific bands in wireless charging technology.

**Author Contributions:** Conceptualization, H.L. and J.Z.; methodology, H.L., X.W.; software, H.L.; validation, H.L., X.W.; formal analysis, H.L. and J.Z.; writing—original draft preparation, H.L.; writing—review and editing, H.L. and J.Z.; supervision, J.Z.; project administration, J.Z.; funding acquisition, J.Z.

**Funding:** This research was funded by the Basic Science Center Project of NSFC under grant No. 51788104, as well as National Natural Science Foundation of China under Grant Nos. 51532004 and 11704216.

**Conflicts of Interest:** The authors declare no conflict of interest.

#### References

1. Veselago, V.G. The electrodynamics of substances with simultaneously negative values of  $\epsilon$  and  $\mu$ . *Uspekhi Fizicheskii Nauk* **1967**, *92*, 517–548. [[CrossRef](#)]
2. Veselago, V.G. Electrodynamics of substances with simultaneously negative values of  $\sigma$  and  $\mu$ . *Sov. Phys. Uspekhi Ussr* **1968**, *10*, 509–514. [[CrossRef](#)]

3. Cui, T.J.; Qi, M.Q.; Wan, X.; Zhao, J.; Cheng, Q. Coding metamaterials, digital metamaterials and programmable metamaterials. *Light Sci. Appl.* **2014**, *3*, e218. [[CrossRef](#)]
4. Silva, A.; Monticone, F.; Castaldi, G.; Galdi, V.; Alu, A.; Engheta, N. Performing Mathematical Operations with Metamaterials. *Science* **2014**, *343*, 160–163. [[CrossRef](#)] [[PubMed](#)]
5. Yang, Y.; Kravchenko, I.I.; Briggs, D.P.; Valentine, J. All-dielectric metasurface analogue of electromagnetically induced transparency. *Nat. Commun.* **2014**, *5*, 5753. [[CrossRef](#)] [[PubMed](#)]
6. Jenkins, S.D.; Ruostekoski, J.; Papasimakis, N.; Savo, S.; Zheludev, N.I. Many-Body Subradiant Excitations in Metamaterial Arrays: Experiment and Theory. *Phys. Rev. Lett.* **2017**, *119*, 053901. [[CrossRef](#)] [[PubMed](#)]
7. Prodan, E.; Radloff, C.; Halas, N.J.; Nordlander, P. A hybridization model for the plasmon response of complex nanostructures. *Science* **2003**, *302*, 419–422. [[CrossRef](#)]
8. Funston, A.M.; Novo, C.; Davis, T.J.; Mulvaney, P. Plasmon Coupling of Gold Nanorods at Short Distances and in Different Geometries. *Nano Lett.* **2009**, *9*, 1651–1658. [[CrossRef](#)]
9. Wu, D.J.; Liu, X.J. Tunable near-infrared optical properties of three-layered gold-silica-gold nanoparticles. *Appl. Phys. B Lasers Opt.* **2009**, *97*, 193–197. [[CrossRef](#)]
10. Park, T.-H.; Nordlander, P. On the nature of the bonding and antibonding metallic film and nanoshell plasmons. *Chem. Phys. Lett.* **2009**, *472*, 228–231. [[CrossRef](#)]
11. Kurter, C.; Tassin, P.; Zhang, L.; Koschny, T.; Zhuravel, A.P.; Ustinov, A.V.; Anlage, S.M.; Soukoulis, C.M. Classical Analogue of Electromagnetically Induced Transparency with a Metal-Superconductor Hybrid Metamaterial. *Phys. Rev. Lett.* **2011**, *107*, 043901. [[CrossRef](#)] [[PubMed](#)]
12. Hentschel, M.; Saliba, M.; Vogelgesang, R.; Giessen, H.; Alivisatos, A.P.; Liu, N. Transition from Isolated to Collective Modes in Plasmonic Oligomers. *Nano Lett.* **2010**, *10*, 2721–2726. [[CrossRef](#)] [[PubMed](#)]
13. Aydin, K.; Pryce, I.M.; Atwater, H.A. Symmetry breaking and strong coupling in planar optical metamaterials. *Opt. Express* **2010**, *18*, 13407–13417. [[CrossRef](#)] [[PubMed](#)]
14. Liu, H.; Genov, D.A.; Wu, D.M.; Liu, Y.M.; Liu, Z.W.; Sun, C.; Zhu, S.N.; Zhang, X. Magnetic plasmon hybridization and optical activity at optical frequencies in metallic nanostructures. *Phys. Rev. B* **2007**, *76*, 073101. [[CrossRef](#)]
15. Verellen, N.; Van Dorpe, P.; Huang, C.; Lodewijks, K.; Vandenbosch, G.A.E.; Lagae, L.; Moshchalkov, V.V. Plasmon Line Shaping Using Nanocrosses for High Sensitivity Localized Surface Plasmon Resonance Sensing. *Nano Lett.* **2011**, *11*, 391–397. [[CrossRef](#)]
16. McPolin, C.P.T.; Marino, G.; Krasavin, A.V.; Gili, V.; Carletti, L.; De Angelis, C.; Leo, G.; Zayats, A.V. Imaging Electric and Magnetic Modes and Their Hybridization in Single and Dimer AlGaAs Nanoantennas. *Adv. Opt. Mater.* **2018**, *6*, 1800664. [[CrossRef](#)]
17. Talley, C.E.; Jackson, J.B.; Oubre, C.; Grady, N.K.; Hollars, C.W.; Lane, S.M.; Huser, T.R.; Nordlander, P.; Halas, N.J. Surface-enhanced Raman scattering from individual Au nanoparticles and nanoparticle dimer substrates. *Nano Lett.* **2005**, *5*, 1569–1574. [[CrossRef](#)]
18. Huang, Z.; Wang, J.; Liu, Z.; Xu, G.; Fan, Y.; Zhong, H.; Cao, B.; Wang, C.; Xu, K. Strong-Field-Enhanced Spectroscopy in Silicon Nanoparticle Electric and Magnetic Dipole Resonance near a Metal Surface. *J. Phys. Chem. C* **2015**, *119*, 28127–28135. [[CrossRef](#)]
19. Alonso-Gonzalez, P.; Albella, P.; Golmar, F.; Arzubiaga, L.; Casanova, F.; Hueso, L.E.; Aizpurua, J.; Hillenbrand, R. Visualizing the near-field coupling and interference of bonding and anti-bonding modes in infrared dimer nanoantennas. *Opt. Express* **2013**, *21*, 1270–1280. [[CrossRef](#)]
20. Moradian, R.; Saliminasab, M. Surface-Enhanced Raman Scattering in Tunable Bimetallic Core-Shell. *Plasmonics* **2018**, *13*, 1143–1151. [[CrossRef](#)]
21. Yang, H.; Yao, J.; Wu, X.-W.; Wu, D.-J.; Liu, X.-J. Strong Plasmon-Exciton-Plasmon Multimode Couplings in Three-Layered Ag-J-Aggregates-Ag Nanostructures. *J. Phys. Chem. C* **2017**, *121*, 25455–25462. [[CrossRef](#)]
22. Park, J.-E.; Kim, S.; Son, J.; Lee, Y.; Nam, J.-M. Highly Controlled Synthesis and Super-Radiant Photoluminescence of Plasmonic Cube-in-Cube Nanoparticles. *Nano Lett.* **2016**, *16*, 7962–7967. [[CrossRef](#)] [[PubMed](#)]
23. Liu, H.; Liu, Y.M.; Li, T.; Wang, S.M.; Zhu, S.N.; Zhang, X. Coupled magnetic plasmons in metamaterials. *Phys. Status Solidi (b)* **2009**, *246*, 1397–1406. [[CrossRef](#)]
24. Hao, F.; Nehl, C.L.; Hafner, J.H.; Nordlander, P. Plasmon resonances of a gold nanostar. *Nano Lett.* **2007**, *7*, 729–732. [[CrossRef](#)]

25. Liu, N.; Giessen, H. Coupling Effects in Optical Metamaterials. *Angew. Chem. Int. Ed.* **2010**, *49*, 9838–9852. [[CrossRef](#)]
26. Liu, X.; Lan, C.; Bi, K.; Li, B.; Zhao, Q.; Zhou, J. Dual band metamaterial perfect absorber based on Mie resonances. *Appl. Phys. Lett.* **2016**, *109*, 062902. [[CrossRef](#)]
27. Guo, Y.; Liang, H.; Hou, X.; Lv, X.; Li, L.; Li, J.; Bi, K.; Lei, M.; Zhou, J. Thermally tunable enhanced transmission of microwaves through a subwavelength aperture by a dielectric metamaterial resonator. *Appl. Phys. Lett.* **2016**, *108*, 051906. [[CrossRef](#)]
28. Bi, K.; Guo, Y.; Liu, X.; Zhao, Q.; Xiao, J.; Lei, M.; Zhou, J. Magnetically tunable Mie resonance-based dielectric metamaterials. *Sci. Rep.* **2014**, *4*, 7001. [[CrossRef](#)]
29. Wu, H.; Zhou, J.; Lan, C.; Guo, Y.; Bi, K. Microwave Memristive-like Nonlinearity in a Dielectric Metamaterial. *Sci. Rep.* **2014**, *4*, 5499. [[CrossRef](#)]
30. Bi, K.; Huang, K.; Zeng, L.Y.; Zhou, M.H.; Wang, Q.M.; Wang, Y.G.; Lei, M. Tunable Dielectric Properties of Ferrite-Dielectric Based Metamaterial. *PLoS ONE* **2015**, *10*, e0127331. [[CrossRef](#)]



© 2019 by the authors. Licensee MDPI, Basel, Switzerland. This article is an open access article distributed under the terms and conditions of the Creative Commons Attribution (CC BY) license (<http://creativecommons.org/licenses/by/4.0/>).